




Feasibility of a Morphing Rocket Nozzle for Thrust Vector Control based on Corrugated Composite Laminates

Alessandro Airoidi¹ · Matteo Boiocchi² · Maurizio Natali³ · Chiara Mirani¹ · Luca Di Pancrazio¹ · Gabriele Consiglio¹ · Pietro Ballarin¹  · Marco Riva¹

Received: 14 September 2022 / Accepted: 25 October 2022 / Published online: 7 December 2022
© The Author(s) 2022

Abstract

The paper presents technological, experimental and numerical studies aimed at the development of a morphing nozzle in composite material with a deformable divergent section, which is designed to control the vector of thrust in rockets without using mechanisms or localized flexible joints. The nozzle design is characterized by corrugated composite walls and longitudinal elements that make possible a separation of load paths involved in bending response, bearing of internal pressures and related force resultants. Mechanical requirements and conditions of pressure, temperature and gas velocity in the morphing part of the nozzle are defined by selecting and investigating two potential application scenarios. Thereafter, both technological aspects and the assessment of mechanical performances are addressed by designing, manufacturing and testing a composite demonstrator with morphing capabilities. A lightweight and flexible thermal protection system is proposed, designed and numerically analyzed. Finally, a virtual demonstrator of the composite morphing nozzle is developed. Results point out the possibility of manufacturing composite elements with axial load bearing capability that may undergo significant bending deformation without failures. The integration of a flexible thermal protection systems leads to a promising concept for the development of innovative morphing nozzle for rocket engine applications.

Keywords Composites · Corrugated laminates · Rocket nozzle · Morphing · Thrust vector control · Manufacturing

1 Introduction

In the field of spacecraft propulsion, several studies demonstrate the possibility of strongly reducing the cost per launch by using innovative architectures [1–4], so to meet the necessities of public and private companies, which are committed to explore and

✉ Pietro Ballarin
pietro.ballarin@polimi.it

¹ Politecnico di Milano, Milan 20156, Italy

² Petroceramics S.p.A., Stezzano (BG) 24040, Italy

³ Università di Perugia, Perugia 06123, Italy

apply the most efficient solutions for a low cost access to space. The active control of the trajectory of a missile or a spaceship, obtained by changing the orientation of the thrust axis, hereafter named thrust vector control (TVC), is one of the most important propulsive requirement which is needed, for instance, to actively control the trajectory to follow a target, or to counter balance the effects of wind gusts. The change of the direction of flight in space, where conventional aerodynamic surfaces are ineffective, can be achieved by altering the thrust vector of the engine or of engines cluster. Therefore, the system of active control of the trajectory of a missile or a spaceship in space flight is a primary means of attitude control, which can significantly affect the complexity and the cost of rocket engine. TVC systems, used both for civilian and military applications, have been implemented on different kinds of aerospace vehicles such as aircrafts, rockets, spacecrafts, satellites, and landers. The space engineers' ingenuity developed many different solutions, which were investigated to achieve TVC functionalities (see for instance [5, 6]) such as the gimbaling of the entire combustion chamber, which represents the most efficient TVC technique implemented on liquid rocket engines [7, 8]. In solid propellant motors a common structural architecture for solid rocket booster is based on the rotation of the nozzle, mounted on a fixed combustion chamber by means of a flexible joint [65]. In one the most successful solutions for the TVC of solid rocket motors in large launchers, a flexible bearing or flexseal is adopted [9–15]. Such an element consists of a toroidal stratified structure made of elastomeric and metallic (or composite) portions of a spherical cap (called shims) which must support the nozzle structure providing, at the same time, the possibility of few degrees of rotation enabling at the same time the thrust orientation modification. Typically, flexible bearing may have from 10 to 20 of such layers [13–15]. Indeed, the flexible bearing is a well-established technology applied to solid rocket motors with angles of rotation such as 7° obtained by using a predictable, though relatively high and variable, actuation force and power [9]. Such joint is a critically loaded element, which must transmit a significant fraction of the thrust to the rocket body and is placed at the end of combustion chamber, in contact with gases at very high temperature and pressure. The necessity to introduce a thermal protection to the joint represents a fundamental additional complication for design and material selection, as well as for maintenance and monitoring effort in case of reusable systems. Despite these technological challenges, such technology has been used in the solid booster of large launchers, as in Space Shuttle and Ariane 5 boosters [9, 16–18].

This work is aimed at presenting a different solution for a low cost TVC system, which is based on the possibility of completely changing the shape of a nozzle made of composite corrugated laminate, so to reduce the technological complexity with respect to a rotational support for a rigid nozzle structure, as in the case of the gimbal and the flexible bearing joints. Such a possibility could lead to the introduction of functional TVC capabilities in a zone subjected to less severe thermal and mechanical loads, both in terms of pressure and thrust, allowing high angles of rotation, with potential lower requirements in terms in actuation force and power. The specific solution considered in this work is developed by exploiting the properties of corrugated composite laminates, following ideas and concepts developed in the field of morphing aeronautical structures, which have been the subject of intense studies by aerospace research in the last decades [19, 20]. In this area, composite corrugated laminates emerged as a promising concept for morphing structures and were originally proposed for the skin of morphing aerodynamic surfaces in [21]. They were subsequently studied and applied by other authors [22–27]. Corrugated shapes are inherently characterized by a strong

anisotropy, with stiffness and strength properties along and normal the corrugation direction that can be different of several order of magnitude [28, 29]. Moreover, composite laminates produced by stacking-up plies of long fiber reinforced plastics offer additional design flexibility due to the possibility of optimizing the lay-up and the orientation angle of reinforcement fibers.

Starting from these considerations, in this work a morphing nozzle with a geometry based on a composite corrugated tube was conceived, reinforced by lateral supports disposed in such a way to carry thrust loads with a minimal influence on the bending requirements. The development of such an element had to face critical issues regarding different areas. In particular, the technological feasibility, the required strength to carry internal pressures and thrust resultant, the development of a flexible and adequate thermal protection system had to be considered. All these aspects are considered in the technological, numerical and experimental activities that are presented in this paper to investigate and preliminary assess the potential of a morphing nozzle for real applications.

The paper is organized in six sections, including this introduction. In the second section, the concept of the morphing nozzle is presented with more details and some possible application scenarios are considered, based on data referred to existing propulsive systems, so to provide a set of realistic dimensional and operational requirements for the feasibility study. In the third section, the technological process to manufacture a reinforced composite corrugated tube is developed. Then, a numerical FEM model of such demonstrator and its experimental validation are presented, with the aim of assessing the real mechanical response of the morphing concept and of validating the numerical approaches that can be used for system design and verification. The fourth section is dedicated to the conceptual development of an adequate thermal protection system. The sizing of such system is carried out following the requirements of the selected application scenarios and solutions are assessed by using thermo-mechanical numerical models. A virtual prototype of the morphing nozzle is finally developed in the fifth section, showing the potential in terms of maximum angle of rotation of the end sections and evaluating the actuation forces required. The overall findings of the research are summarized in the sixth conclusive section.

2 Corrugated Morphing Nozzle Concept and Application Scenarios

In the solution proposed in this paper, the control of the vector of thrust has to be achieved without using any mechanism or moving part. Such goal can be accomplished by exploiting the mechanical properties of corrugated structures based on carbon-fiber composite materials. Accordingly, it is proposed to use a corrugated composite tube in the external structure of the final part of the nozzle, which must be protected from the internal gases by using a flexible thermal protection system (FTPS). A sketch of the resulting thermally protected morphing nozzle is shown in Fig. 1.

2.1 Main Issues, Adopted Solutions, and Expected Advantages

The concept sketched in Fig. 1 presents some significant design challenges, which are hereby summarized:

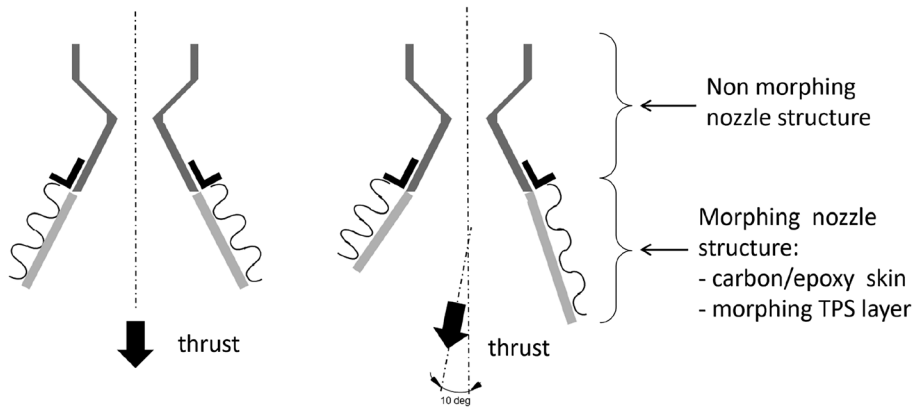


Fig. 1 Sketch of the proposed TVC system based on the corrugated morphing nozzle concept

- i) the transmission of thrust loads to the structure of the rocket, without excessive deformation or collapse of the corrugated structure;
- ii) the resistance to the action of the pressure loads exerted by the exhaust gas during their expansion
- iii) the necessity of protecting such a thin corrugated laminate from the hot exhaust plume;
- iv) the interaction between the gas flow and the internal corrugated shape, which is expected to have a not negligible detrimental effect on thrust efficiency;

Issues i) and ii) conflict with the necessity of maximizing the deformability of the morphing part of the nozzle, in order to achieve high angles of rotation with the lowest actuation force. For the transmission of force, a system of lateral stiffeners was included in the nozzle structure. These elements carry the axial loads without opposing to the bending of the tube about a pre-defined axis. The nozzle can be manufactured by assembling different modules with mutually perpendicular bending axes so that, by combining the allowable rotations, a generic orientation can be achieved. This structural concept is assessed in the paper by developing a demonstrator based on a cylindrical geometry, which is shown in Fig. 2. The morphing structure of the demonstrator consists of two modules, each one reinforced by a pair of thin lateral stiffeners. The mechanical and technological issues related to such structural concept are investigated in Sect. 3 of the paper, which is focused on the design, manufacturing, modelling and testing of the demonstrator sketched in Fig. 2.

Considering the protection from thermal loads, related to issue iii) in the previous list, the solutions proposed are based on the internal flexible thermal protection system (FTPS), which can morph together with the external structure. Such an internal FTPS should also provide a smooth internal surface, thus eliminating undesired drag effects on the internal flows, thus addressing the aforementioned issue iv). The internal FTPS solution and its integration in the nozzle structures is presented in detail in Sect. 4, considering the properties of ablative and insulating materials typically used in space applications.

Overall, the experimental, technological and numerical activities were performed to develop a preliminary design study, so to investigate the potential of the concept, which is expected to provide a rocket thrust vector control with a series of potential advantages that are hereby summarized:

- possibility of achieving high angle of rotation of the end section without failure;
- reduction of the additional weight and complexity of the TVC system, thanks to absence of mechanisms, critical flexible joints and reduction of actuation forces;
- reduction of the cost of the propulsive system, as a consequence of complexity reduction;
- possible limitation of the forces required for actuating the rotation;
- possibility to introduce some elements of the potential for reusability, since the low-cost terminal part of the nozzle can be removed without requiring the replacement of other structurally critical and expensive parts of the assembly.

2.2 Definition of Reference Data for Possible Application Scenarios

The design of the morphing nozzle was conducted considering real-world requirements and actual technological challenges. A survey led to define two promising types of application scenarios: small rocket size engines with relatively low thrust and temperatures in the nozzle terminal parts and medium size engines with a limited firing time. More specifically, two possible application scenarios (AS) have been identified: a 3 kN liquid monopropellant thruster (MR-80B MLE, Aerojet rocketdine – AS1) and a 32 kN solid propellant motor (Orbital ATK Orion 38 – AS2). The main propulsive data for these original chemical propulsion systems are listed on Table 1.

The MR-80B MLE (AS1) is a liquid rocket engine for a planetary lander with a single nozzle configuration, which is a derivation of the multiple-nozzle configuration of the MR-80 engine used for the two Viking missions to Mars in 1976 [30, 31]. In such a configuration, no TVC was provided, but the thrust directionality was obtained by regulating the thrust of single engine in a six-thruster configuration. The AS2 is represented by the Orion 38 solid propellant engine, which was developed as a third stage for the Pegasus launch vehicle incorporating a ± 5 deg vectorable nozzle. The reported propulsive data are available in [32].

The NASA CEA2 program [33] was used to calculate the values of temperature in combustion chamber, considering a composition of the HTPB-based solid propellant, with 19% by mass of aluminum powder. Calculation was performed by imposing the requirements (average chamber pressure, expansion ratio, propellant composition) reported in [32, 34]. The knowledge of temperature in combustion chamber allowed an evaluation of the operational conditions of the nozzle, which represent a reference for the structures and the TPS of the morphing nozzle. It is worth noting that the morphing structure is limited to the terminal part of the nozzle, where temperatures and pressures can be significantly lower than those in throat or in combustion chamber. A computation of the gasdynamic expansion of the exhausts was performed under the assumptions of 1-D nozzle, isentropic flow and frozen chemistry [5], by implementing the resulting simplified analytical model in a Matlab[®] script. The results are reported in Fig. 3, where the pressure (Fig. 3A), the temperature (Fig. 3B), and the exhaust speed (Fig. 3C) are given as a function of the normalized expansion ratio for AS1 and AS2. A dashed vertical line is drawn in correspondence of a value of the expansion ratio which corresponds to the beginning of the morphing part of the nozzle.

Fig. 2 Design of the technological demonstrator; structural concept (A) and corrugated profile adopted (B) ▶

3 Manufacture, Modelling and Testing of a Corrugated Demonstrator

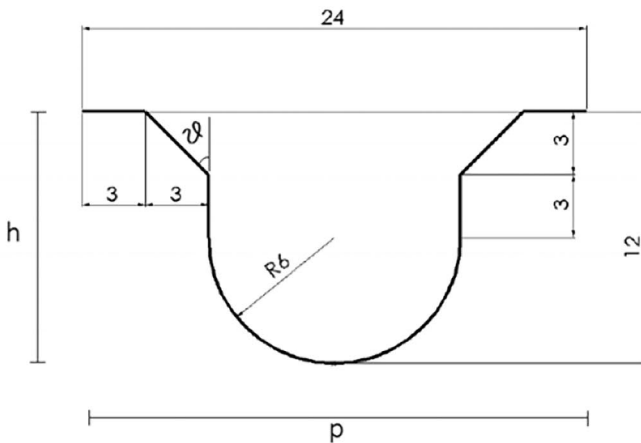
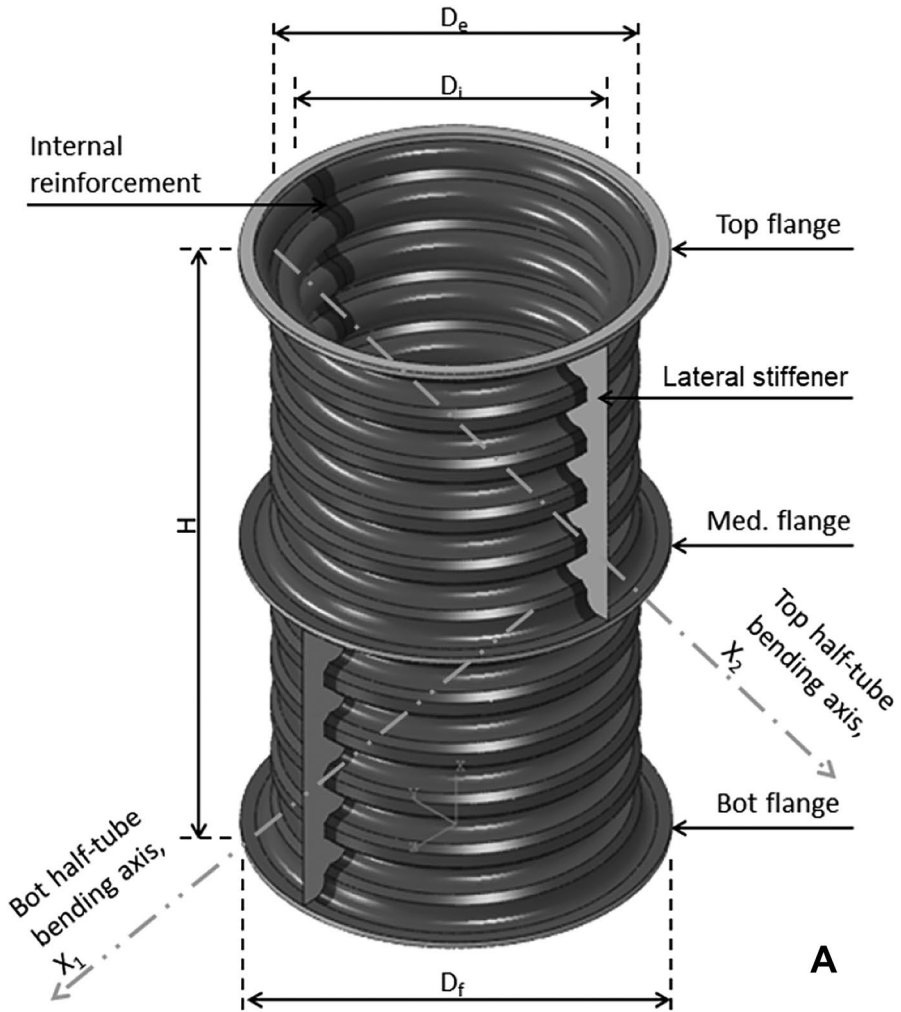
3.1 Design and Material Selection for the Simplified Technological Demonstrator

The development of the corrugated cylindrical demonstrator, presented in Fig. 2, represents a significant milestone to evaluate the technological feasibility and a first experimental assessment of the mechanical functional concepts of the morphing nozzle. The tube manufacturing required the production of a double-curved surface with composite plies and the lamination technology was adopted, assuming that the drapability of the composite plies was adequate and that the required curing pressures could be uniformly exerted. Production and integration of the lateral stiffener elements also represented a technological issue.

On the basis of technological considerations, an internal diameter D_i of 120 mm was selected for the demonstrator shown in Fig. 2A. Such diameter can be considered representative of the AS1 engine, which has an exit diameter of 154 mm.

Previous experimental activities on corrugated composite laminates drove the selection of the material and of other geometrical parameters for a first technological trial [27]. The chosen nominal profile is shown in Fig. 2B, and has a period, p , of 24 mm and a height, h , of 12 mm, with a rounded shape to simplify lamination on the double-curved surface. As a consequence, the external diameter D_e of the tube results of 144 mm. A flange diameter, D_f , of 160 mm was adopted. The modules of the demonstrator were designed to achieve a total length of 273 mm, similar to the nozzle length in AS1. The material selected for tube production was a carbon fabric ply HexPly® M49, a plain weave fabric with a cured ply thickness of 0.22 mm. Material properties were obtained by characterization tests, performed by testing $[0/90]_{2s}$ and $[+45/-45]_{2s}$ coupons in agreement with ASTM standards [35, 36]. The average elastic constant resulted $E_{11} = E_{22} = 64,602$ MPa, $\nu_{12} = 0.052$, $G_{12} = 4043$ MPa. These data were consistent with those presented in the material datasheet given by the producer [37]. Considering the projection of tube longitudinal axis as a reference direction on the corrugated laminate, a $[+45/-45]$ lamination sequence was adopted for the demonstrator, to maximize tube bending compliance.

The lateral stiffeners were designed with a 1 mm thick core made of a polyamide polymer (PA2200), which was produced by means of a Selective Laser Sintering 3D-printing process (Fig. 4). Material has a Young Modulus of 1600 MPa, a Poisson's ratio of 0.3, and a Vicat softening temperature of 163 °C [38]. Such polymeric cores, shown in Fig. 4B, were coated in the final assembly process by using two plies of the same carbon fabric used for the tube (Fig. 4C), to increase the stiffness and the critical buckling loads and enhance compressive load carrying capability. Such a polymeric material was chosen considering the scope of the demonstrator manufacturing and provides an assessment of the potential of the 3D-printing processes for the production of the most complex geometrical parts of the nozzle. Moreover, the softening temperature of the polymer used was adequate to withstand to a secondary bonding process for the final assembly of the demonstrator. Actually, for higher mechanical performances and service temperature, metallic parts can be taken into consideration also adopting and additive manufacturing technology.



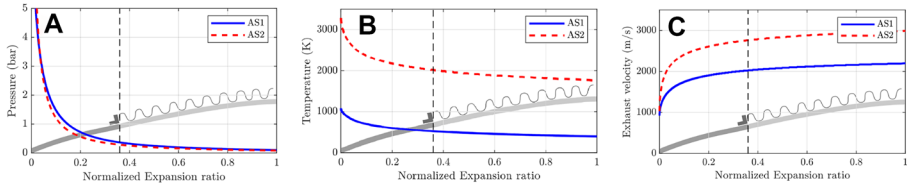


Fig. 3 Operational conditions of the nozzles in application scenarios: pressure (A), temperature (B), and exhaust velocity (C) vs. normalized expansion ratios

3.2 Technological Process

The technological process set up to manufacture the demonstrator consisted of a first step for the production of four corrugated semi-tubes, which were subsequently joined in a secondary assembly process. Such a second step also involved the application and the coating of the 3D-printed polymeric cores of the lateral stiffeners. Finally, in a third step, the modules were joined together in a procedure carried out at room temperature.

In the first step, a pre-shaping procedure was developed to achieve the double curved corrugated surface. Two rectangular elastomeric forming pads were manufactured, by using a soft silicon rubber (RECKLI™ Si Compound 20 with a shore A hardness of 20) with one side shaped as the corrugated profile to be obtained (Fig. 5A). The fabric plies were laminated and pressed within the pads and then wound around a circular mandrel (see Fig. 5B). Subsequently, the pre-shaped laminate was applied on an aluminum alloy mold and pressed against it by using a third elastomeric pad, as shown in Fig. 5C. The assembly was closed inside a vacuum bag and cured in autoclave at 120 °C. A pressure value of 8 bars was selected to achieve a good surface finish and limit to minimum values the discrepancies with the nominal dimensions. One of the produced elements is shown in Fig. 6.

Once four corrugated elements and the lateral stiffeners were produced, the assembly of each module was carried out. The two halves of the module were positioned around a cylindrical a mandrel with a diameter slightly lower than the internal diameter of the corrugated tube (see Fig. 7A) to be connected by means of a double overlap junction. The external overlap consisted of the corrugated flange of the polymeric

Table 1 List of propulsive parameters of the selected engines

Propulsive data	AS1 MR-80B MLE	AS2 Orbital ATK Orion 38
Propellant	Hydrazine	HTPB/AP/Al
Thrust, N	3000	32,200
Combustion chamber Pressure, Bar	20.0*	39.4**
Combustion chamber Temperature, K	1221*	3482**
Expansion ratio	16.7	49.3
Total firing time, s	560	67.7
Single firing, s	214	67.7
Nozzle exit diam., mm	154	526
Nozzle div. Length, mm	218	842
TVC, deg	Multiple engines	± 5

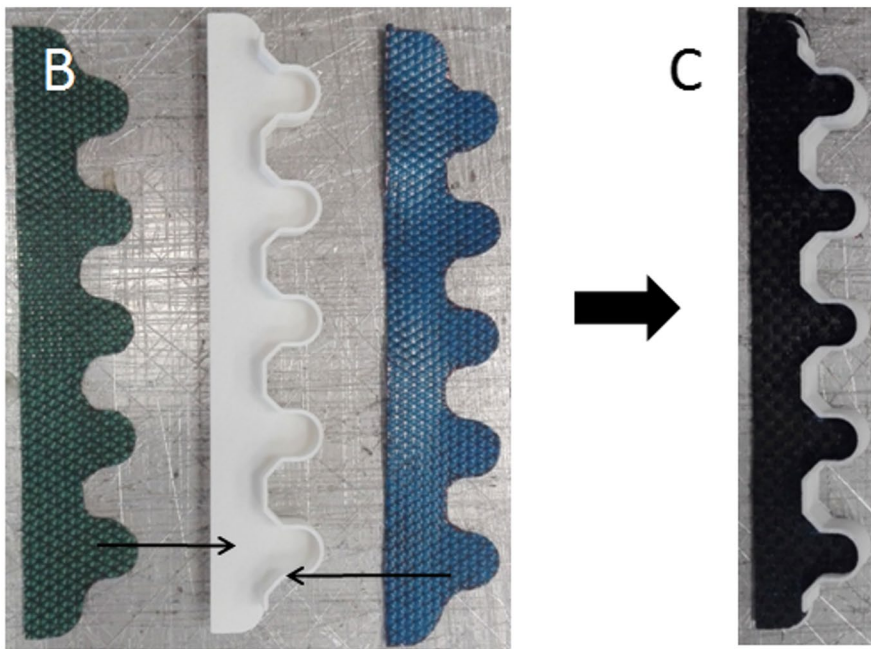
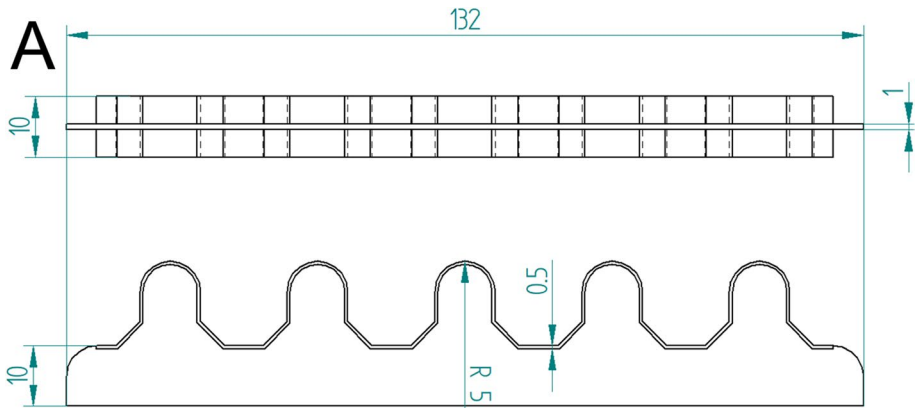


Fig. 4 Design of Polyamide lateral stiffeners (A), 3D-printed element with carbon fabric reinforcement plies (B) laminated element to be cured in the final assembly process (C)

lateral stiffeners, and the internal overlap was obtained by co-bonding additional fabric plies to the inner surfaces, shown in Fig. 7B. Both the polymeric flange and the additional plies were bonded to the corrugated tubes by using a film of 3 M™ Scotch-Weld™ AF-163-2 k structural adhesive. The exertion of pressure was aided by internal stripes of silicon rubber, which were inserted between the composite tubes and the mandrel, visible in Fig. 7B. The tube halves and the polymeric cores were positioned on an assembly

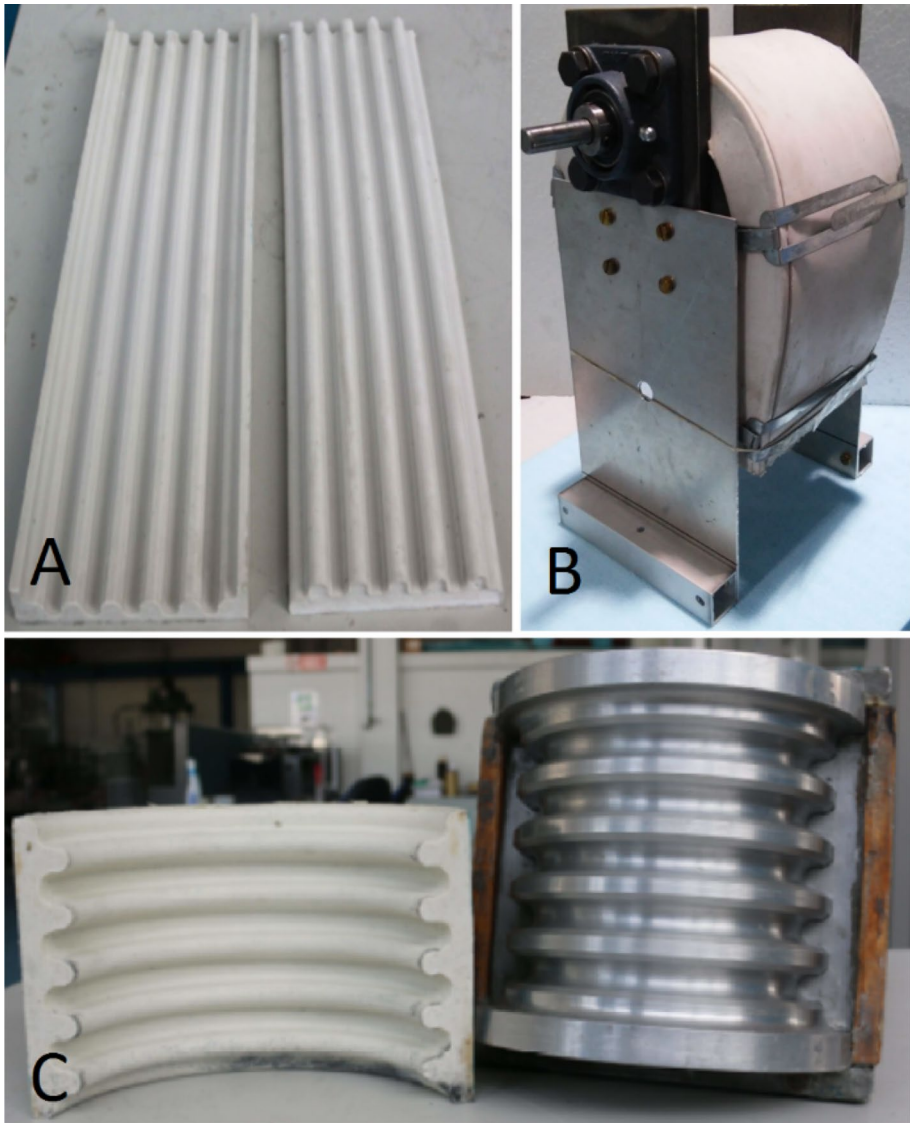


Fig. 5 Elastomeric pad for pre-shaping (A), pre-shaping of composite laminate (B), elastomeric counter-mold for autoclave curing and metallic mold (C)

fixture shown in Fig. 7C to accomplish a second curing cycle at 120 °C, where carbon fabric reinforcing plies were also applied to the stiffeners according to the design shown in Fig. 4.

In the final step, the modules produced were eventually connected together by bonding them to an interface aluminum ring having a thickness of 3 mm by using a room temperature curing bi-component epoxy adhesive. The complete demonstrator is shown in Fig. 7D.

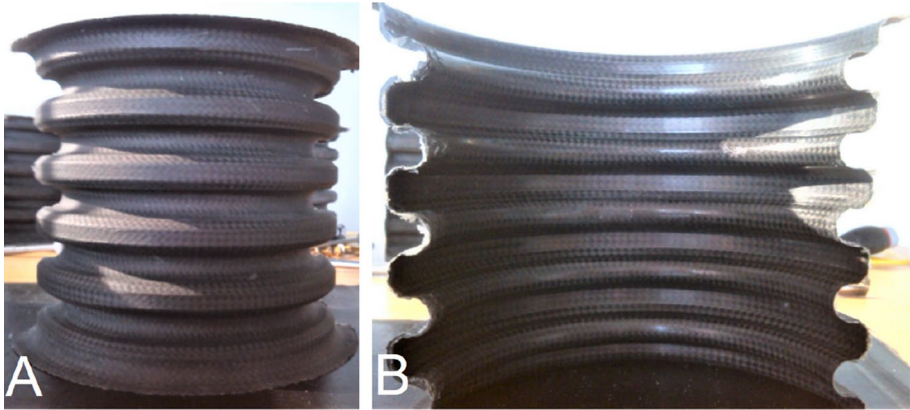


Fig. 6 Example of corrugate element produced; external surface (A), internal surface (B)

3.3 Development of a Numerical Model and Bending Analysis

The expected mechanical performances of the cylindrical demonstrator were numerically evaluated by developing a finite element model, which was solved by using the Simulia/Abaqus Standard code. Conventional bi-linear shell elements (*S4R* type [39]) were used to represent both the corrugated tube and the lateral stiffeners. For the connection rings, indicated in Fig. 2A as *top*, *med* and *bot* flange, continuum shell elements (*SC8R* type [39]) were used. All the elements had a characteristic length of 1.5 mm and the FE model had a total number of 106,744 elements and 625,200 DOFs. The shells representing the corrugated tube were characterized with a lamination sequence [+45/-45] of 0.22 mm thick carbon fabric plies having the elastic properties reported in sub-Sect. 3.1. Laminated shells were used also for the stiffeners, with a sequence [CF 0/PA/CF 0], which included a central ply with the characteristic of the Polyamide (PA) material ($E=1800$ MPa and $\nu=0.3$ [38]). The double overlap junction zone, in correspondence of the lateral stiffener elements, was modelled by adding three plies of



Fig. 7 Module assembly: application of overlaminates between the tube halves (A), internal stripes of silicon rubber for pressure application (B), fixture for the assembly process (C) and produced demonstrator (D)

carbon fabric (internal overlap) and one ply with the characteristics of PA material the lamination sequence of the shell elements.

Bending analyses were performed to evaluate the deformed shape and the state of stress for rotation in different directions. Risk of failure was estimated by considering that the characterization tests performed on the carbon fabric material provided a strength in the fibre reinforcement direction higher than 800 MPa and a maximum in-plane shear stress that exceeded 100 MPa, which was evaluated by testing $[+45/-45]_{2s}$ coupons. A rigid body was created with all the nodes belonging to the upper flange, and a rotation of 7° was imposed along two axes X_1 and X_2 , which lay in the planes of the lateral stiffener elements of the lower and upper module, and are shown in Fig. 2A. The nodes of the lower flange were constrained to the fixed reference frame. The contours presented in Fig. 8 are referred to the stress components σ_{11} and τ_{12} for the rotation about the X_2 axis. The stress in fibre directions remained in the range $-121 \text{ MPa} \div +127 \text{ MPa}$ in the corrugated core and $-58 \text{ MPa} \div 52 \text{ MPa}$ in the stiffeners, without evidencing risks for the structural integrity. The absolute value of shear in material axis, τ_{12} , was 45 MPa in the corrugated core, which was below the average strength of the coupons, though quite close to the linearity limit. The moments required to achieve the 7° rotation was 21.4 Nm, identical for both bending cases.

3.4 Bending Tests and Validation of the Numerical Approach

Experimental tests were performed to verify the morphing concept and to correlate the numerical results with the experiments, so to validate the numerical approach for subsequent studies.

The complete corrugated tube was tested by using the experimental rig shown in Fig. 9. Tests were performed by measuring the deflection of the structure under the action of a bending moment applied along different bending axes. Load application was carried out by using calibrated masses (0.5 to 2 kg) placed at 500 mm of distance from the tube longitudinal axis, at the end of a 1 m long metallic beam with a weight of 1 kg, shown in Fig. 9, which was attached to the flange at the top of the tube. The response was experimentally assessed by applying masses having increasing values and varying the orientation of the

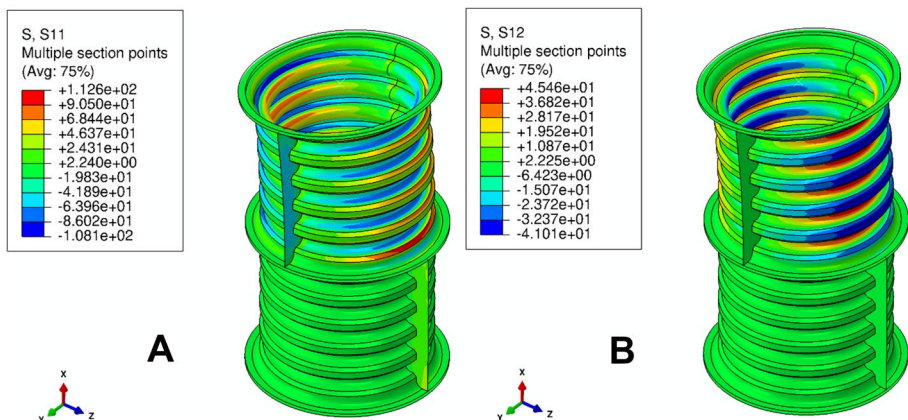


Fig. 8 Contour of σ_{11} (A) and τ_{12} (B), both in MPa, in a bending analysis (rotation of 7° about X_2 axis)

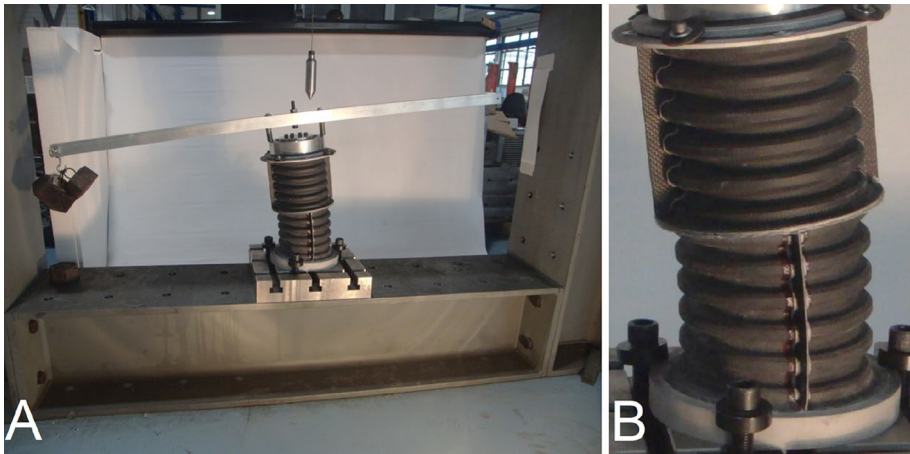
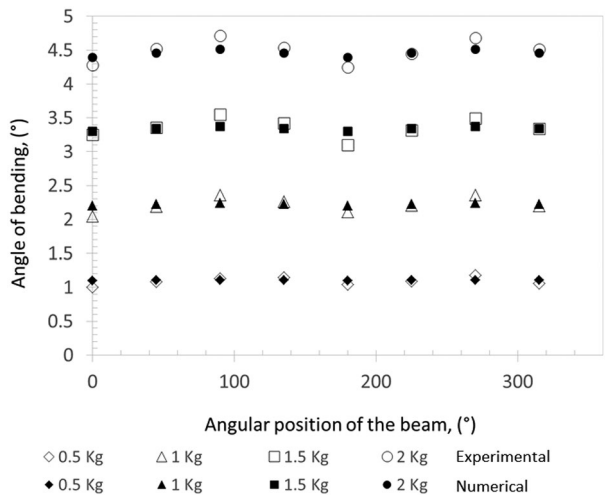


Fig. 9 Experimental bending test: lay-out with 2 kg of mass loading (A), magnification of the bending of the sample (B)

beam with respect to the plane containing the upper lateral stiffener element, at different angular positions equally spaced of 45°. The obtained inclinations of the beam were measured by using a digital inclinometer and are shown by the white symbols in Fig. 4. It can be observed that the response is approximately linear and rotation angles up to 4.7° were obtained without any indication of damage. Rotations were quite constant with the variation of moment direction, with the exception of those obtained when the beam was rotated at 0° and 180° and is thus aligned with the upper lateral stiffeners, which probably introduced a stiffening effect. However, maximum discrepancies between the rotation angles with a mass of 2 kg were below 10% with respect to the average values.

The tests were analyzed by applying proper boundary conditions to the numerical model described in sub-Sect. 3.3 The numerical results are compared with the experimental ones in Fig. 10. Numerical results also exhibit a variation with the moment orientation, though such phenomenon is less apparent than in the experimental data. Overall, the correlation

Fig. 10 Experimental and numerical deflection angles in bending tests



can be considered acceptable, taking into account all the possible imperfections introduced in the manufacturing process which were not represented in the numerical model. Considering the average experimental rotations with a mass of 2 kg, the bending stiffness of the demonstrator results of 2.18 Nm/deg.

4 Design and Analysis of a Flexible Thermal Protection System

4.1 Material Selection for the TPS

Manufacturing, testing and numerical models of the demonstrator indicated the feasibility of the corrugated composite nozzle concept from the technological and mechanical standpoint. However, the internal surface of the nozzle is required to be protected by the excessive temperature or the direct contact with the exhaust gases, and to present a smooth surface for their flow, in order to maximize propulsive efficiency. These requirements should be met without increasing excessively the bending stiffness, so to minimize the loads required for actuation.

The limit temperature for the walls of the nozzle can be set to the glass transition temperature, T_g , of the composite plies constituting the corrugated laminate. Actually, carbon-epoxy reinforced fabric plies typically used in aerospace field can exhibit a T_g in the range of 170 °C ÷ 180 °C or higher [40], with even better mechanical properties than those of the material used for the demonstrator. Therefore, such temperature level represents a basic requirement for the TPS integrated in the nozzle. Moreover, an elongation at failure of at least 10% and a low stiffness were considered additional requirements for the TPS material selection, due to the large deformation achieved by the corrugated structure during TVC operations.

A survey of the solutions adopted in rocket propulsion [41–51] points out that the basic ingredients of the FTPS system for the morphing nozzle concept could be represented by two classes of materials: cork-based and EPDM-based (Ethylene Propylene Diene Monomer) compound formulations.

For applications in the space propulsion field, a mix of cork granule (70% in weight) and of a special thermoset phenolic binder was developed for high heat resistance [43–45, 52]. The properties listed in Table 2, taken from [45, 52, 53], exemplify the combination of

Table 2 Main physical and thermal properties of the materials involved in the design of the FTPS

Physical property	Phenolic/cork P45[43, 45, 52, 53]	EPDM compound [47, 51]	Hybrid EPDM-based composite[49]	Honeycomb[56]
Density, ρ , g/cm ³	0.320	0.98/1.1	1.239	0.0977
Thermal conductivity, k , Wm ⁻¹ K ⁻¹	0.060	-	0.178	5.863
Specific heat, C_p , JKg ⁻¹ K ⁻¹	2500	-	1691	893
Ablation rate, mm/s	0.06–0.25	0.09	0.006	N/A
Young modulus (MPa)	18.0	16.0	-	See Table 3
Poisson's ratio	-	0.45	-	See Table 3
Elongation	30%	96.7%	12.1%	> 10%

low density, low thermal conductivity, stiffness and high maximum elongation (30%) that can be achieved. The studies reported in [43, 44] indicates that the major pyrolysis reaction and char formation for phenolic cork material occurs at about 750 K, when heated under nitrogen or air at atmospheric pressure. These values indicate the possibility of adopting a layer of phenolic cork as FTSP in AS1, where the maximum temperature in the deformable part of the nozzle is lower than 550 K (see Fig. 3B), although such a temperature level is close to degradation limits for phenolic resins.

In the morphing part of the nozzle for scenario AS2, the temperature reaches 2000 K, and a different concept must be considered to protect the nozzle structure. A flexible ablative layer made of EPDM elastomer can be considered, since it is normally adopted in combustion chambers (around the igniter, the motor case and the aft dome) of solid rocket motors. EPDM-based compounds are used typically in the presence of higher pressure, temperature, but lower velocities than those that characterize the terminal sections of the nozzles [46, 47, 54]. The ablation mechanism in EPDM is characterized by the formation of char on the surface of the EPDM-based insulation materials exposed to the hot exhaust gases. A reference temperature for the char formation of EPDM based ablatives can be set at about 800 K, when the layer is heated in nitrogen and air [46, 47, 54]. Several types of filler, such as carbon fibres, silica, asbestos, cork powder, and aramid fibres are used to reinforce the EPDM rubber and thus to improve ablative efficiency and the structural integrity of EPDM-based TPS [50], since they reduce to char removal under the action of gas flow. The thermo-mechanical properties of a conventional EPDM-based compound used as ablative layer are reported in Table 2, where an ablation rate of 0.09 mm/s is reported. Properties are taken from [47] except the Young modulus, which is the highest initial slope of the stress vs. strain response of filled and unfilled EPDM compounds, reported in [51]. Different types of reinforcements such as chopped carbon fibres, Kevlar pulp and ammonium polyphosphate were combined in [49], achieving an ablation rate as low as 0.006 mm/s, with an elongation at failure of about 12%. The properties reported in [49] for such material have been included in Table 2 (Hybrid EPDM-based composite).

4.2 Integration of the Flexible Thermal Protection System in the Nozzle Internal Surface

The integration of the FTSP in the corrugated nozzle is an engineering challenge to be considered and has to take into consideration the requirement related to the smoothness of the internal surface. A lightweight solution can be based on the concept presented in [27, 28], where it is described the technological and experimental assessment of a corrugated morphing skin for aeronautical application, based on the integration of a smooth and aerodynamically efficient elastomeric cover on corrugated laminates. Following the approach proposed in [27], honeycomb stripes are inserted in the “valleys” of the corrugation to sustain a flexible layer, so to obtain the configuration sketched in Fig. 11A. According to the experimental and numerical results reported in [27], honeycomb must be connected to the elastomeric layer, but not glued to corrugated walls and the bottom of the stripe is simply in contact with the corrugated composite. For the application of this concept to the current study, an aluminum honeycomb CR-III – 1/8 – 5052 – 6.1P, produced by Hexcel, was selected for the FTSP of the morphing nozzle, with the thermal properties that are reported in Table 2. The mechanical properties of the honeycomb, taken by producer datasheet [56], are reported in Table 3, where the axis 3 is considered along the cell axis, The properties

Table 3 Mechanical properties of the honeycomb selected to support the FTPS

E_{33} (MPa)	$E_{11}=E_{22}$ (MPa)	ν_{12}	$\nu_{13}=\nu_{23}$	G_{12} (MPa)	G_{13} (MPa)	G_{23} (MPa)
1654	0.01	0.3	0.0001	0.0038	675	282

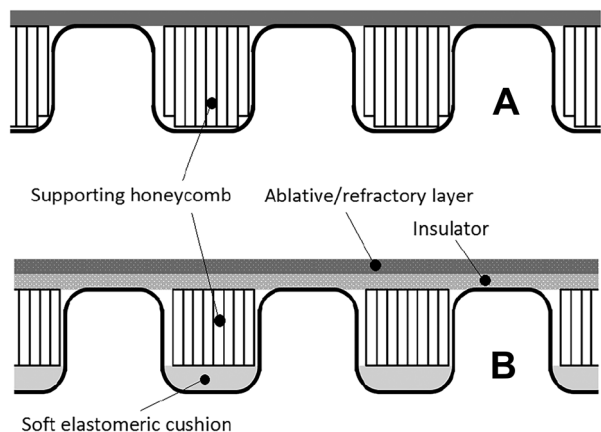
along the in-plane directions (axes 1 and 2) are assumed very small and have a negligible influence of the mechanical performance of the system.

The experiments and the analyses conducted in [27] showed that the elastomeric layer supported by the honeycomb expands and contracts following the deformation of the corrugated without large wrinkles. However, when the corrugated laminate is stretched, the bottom of the valleys bends and tends to push the honeycomb upwards. In the present application, due to high thickness of the protective layer and to the effect of internal pressure field, such phenomenon may lead to stiffen the overall system. This was verified during the set-up of the numerical model of the complete nozzle, presented in the subsequent Sect. 5. Accordingly, the interposition of a soft layer of silicon rubber between the corrugated valley and honeycomb was included in the design of FTPS, shown in Fig. 11B. The elastomeric material used in [27] was considered for such application.

4.3 Thermal Analyses in the Considered Application Scenarios

The FTPS conceived in the previous subsections was dimensioned for both AS1 and AS2, by considering the material properties listed in Table 2 and taking into account the temperatures and the velocities of exhaust gases at the beginning of the corrugated section of the nozzle, provided in Fig. 3. The design hypotheses were verified by means of a thermal transient analysis performed on a finite element model of the simplified square-shaped geometry shown in Fig. 12. The homogenized honeycomb, the silicon rubber cushion, and the FTPS material were modelled by using solid elements with a typical length of 1 mm. Such internal mesh is merged with a mesh of shell elements that represents the composite laminated laminate, for a total number of about 40,000

Fig. 11 Integration of FTPS in the corrugated laminate: initial concept (A) and ablative/insulator solution with an interposed elastomeric cushion (B)



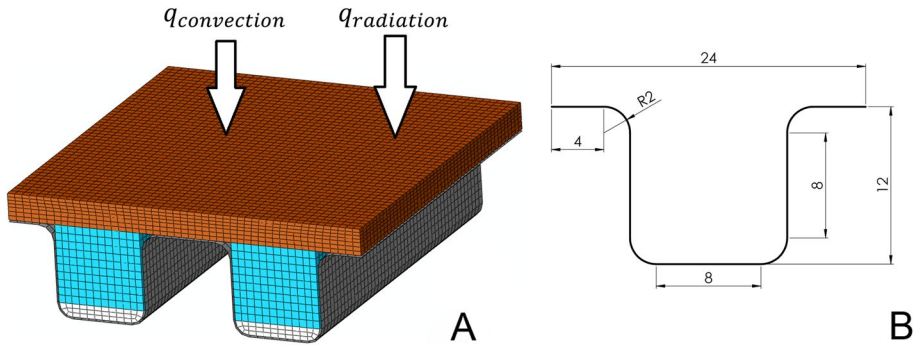


Fig. 12 Representative model for thermal analyses (A) and geometry of the corrugation (B)

elements and 62,000 degrees of freedom. Thermal properties of the material listed in Table 2 have been used to characterize the solid element of the model, while a thermal conductance of $0.870 \text{ Wm}^{-1}\text{K}^{-1}$ and a specific heat of $935 \text{ Jkg}^{-1}\text{K}^{-1}$ were considered for the carbon fabric material [55].

Analyses have been performed by imposing the boundary conditions represented by the internal heat exchange with the exhaust gases and the radiation between the composite nozzle and the external environment, consisting of two contributions, as sketched in Fig. 12A.

The expression of the heat flows at the internal surfaces, related to convection and radiation, are given in Eqs. (1) and (2), respectively.

$$q_{convection} = h_i(T_{gas} - T_{FTPS}) \tag{1}$$

$$q_{radiation} = \alpha\sigma(\epsilon_{gas}T_{gas}^4 - T_{FTPS}^4) \tag{2}$$

The coefficient of forced convection between the internal gases and the FTPS surface was formulated as in Eq. (3):

$$h_i = Nu \cdot k/D \tag{3}$$

where k is the thermal conductivity of exhaust gases, which was set to $0.32 \text{ Wm}^{-1}\text{K}^{-1}$ for hydrazine in AS1 [57] and to $0.535 \text{ Wm}^{-1}\text{K}^{-1}$ for aluminized solid propellant in AS2 [58], D is the diameter of the nozzle in the considered section, Nu is the Nusselt number, which depends on laminar or turbulent regime of the gas flow. For Reynolds number, Re , lower than 2300, the flow is considered laminar and Nu is equal to 4.36, whereas for Re higher than 2300 the flow is turbulent and Nu depends on Reynolds number and Prandtl number, Pr , according to the relation given in Eq. (4) [55].

$$Nu = 0.23Re^{0.8}Pr^{0.3} \tag{4}$$

The radiative heating resulting from the exhaust gases was considered negligible for hydrazine, due to low wall temperature [5] in AS1. For the solid propellant in AS2, expression given in Eq. 2 was adopted. In the formula, σ is the Stefan-Boltzmann constant, α is the surface absorptivity, set at 0.9 under the assumption of grey body, and ϵ_{gas}

is the emissivity of the exhaust gases which was computed according to the expression given in Eq. 5 [59] at the considered nozzle section of diameter D :

$$\epsilon_{gas} = 1 - \exp(-3.972n_{Al}\rho_b D/32) \quad (5)$$

where n_{Al} is the percentage in mass of aluminum content in the propellant and ρ_b is the gas bulk density.

The model was used to verify three design hypotheses for the FTSP. In particular, for AS1, a purely insulating phenolic cork layer of 3.5 mm was chosen, whereas for AS2 two possibilities were analyzed. In the first case (AS2/A), a layer of EPDM compound was considered, with a thickness of 6.3 mm, which was evaluated considering the firing time presented in Table 1 and the ablation rate of 0.09 mm/s presented in Table 2. A second version (AS2/B) is presented considering 1 mm thick layer of the hybrid EPDM-based composite reported in Table 2, with a significantly lower ablation rate (0.006 mm/s) and an insulating layer of 3.5 mm of Phenolic Cork.

A transient was analyzed by imposing initial temperatures to the nozzle structures and a constant temperature, T_{gas} , at the internal boundary, for the whole firing time. Relevant data are reported in Table 4. Without detailed data regarding the mission and the external insulation, the initial temperature of the nozzle structure were set to a reasonable value. The initial temperature for AS2 was set to 873.15 K (600 °C), a value that took into account the temperature of char formation in the EPDM material, as discussed in Sect. 4.1. A conservative assumption was adopted considering the heat exchange of the external surface of the nozzle with the external environment, which was neglected.

The contour reported in Fig. 13A and B are referred to the plot of the temperature increment with respect to initial temperature at the end of the transient analyses for the cases AS1 and AS2/A, respectively.

The analyses indicate that all the three FTSP system obtain promising results in terms of insulation capabilities, since the maximum temperature reached by the composite laminate during the firing time is below the level of 180°, as presented in Fig. 13C. In particular, for the cases AS2/A and AS2/B, the temperature remained lower than 100 °C at the end of the firing time. Such result is promising for the possibility of fulfilling the imposed requirements also considering the uncertainties related to material properties and the progressive reduction of the ablative layer but also, on the other hand, the possible adoption of composite materials specially developed for high temperature applications.

Table 4 Analyses for preliminary sizing of FTSP and max numerical temperature

Scenario	Initial Temp. (K)	EPDM thickness (mm)	Cork Thickness (mm)	Exhaust Temp. (K)	Firing Time (s)	Max Final Temp. (°C)
AS1 3.5 mm Cork	293	0	3.5	520	214	175.3
AS2/A 6.3 mm EPDM	293	6.3	0	873.15	67	81.0
AS2/B 3.5 mm Cork + 1 mm EPDM	293	1.0	3.5	873.15	67	104

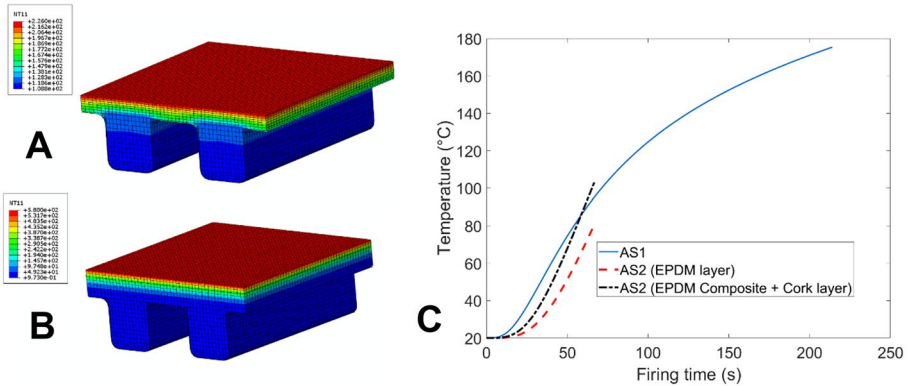


Fig. 13 Contour of temperature increment for AS1 (A) and AS2/A (B) at the end of the transient, and evolution of temperature on the composite plies for the AS1, AS2/A, and AS2/B cases

4.4 Motivation and Guidelines for Alternative Innovative FTSP Configurations

The FTSPs proposed and analyzed in the previous subsection were based on insulating and ablative layers made of materials that are traditionally used in rocket propulsion. However, recent technological advancements should be considered to increase the effectiveness of the morphing nozzle concept proposed in this paper. Actually, the properties of the Hybrid EDPM based composite reported in [49] are particularly promising to develop thin and flexible ablative layers with optimal ablation properties and relatively high elongation at failure. The properties reported for this material were included in Table 2 and considered in the AS/B case to verify the insulating properties of the FTSP, but it should be observed that the formulation is characterized by high filler content, which is expected to increase the stiffness of the material. Unfortunately, stiffness values are not indicated in [49], though they should be known with accuracy to evaluate the validity of the morphing concept.

An issue that should be carefully taken into account is represented by the risk due to the erosion of the proposed heat shields, associated to the loss of charred material due to the shear stress exerted by the supersonic flow in the divergent region of the nozzle, especially in the presence of alumina particles. For the cork-based material, it is known that during the exposure to a harsh environment the charred material tends to expand and crack and, as a result, tends to be removed in presence of strong shear stresses induced by the combustion gases. The erosion resistance of phenolic/cork based ablatives can be increased using additional fillers in the baseline formulations such as chopped fibres and char enhancers. However, it should be observed that operational temperatures in AS1 are quite low and that in AS2/B the cork-based insulation layer is protected by the ablative EPDM layer.

For AS2 scenarios, the presence of high temperatures and gas exhaust velocities could be critical for the erosion of ablative material. The specific conditions and requirements of the nozzle concept under study require an experimental assessment and could lead to the development of ad hoc formulated flexible protective layers, such as the one conceived for inflatable thermal shield presented in [60]. Innovative solutions for the nozzle protection could also be developed by using ablative/refractory and insulating layer made of fiber pre-forms. A first promising candidates is represented by the braided performs i.e. tubular

sleeving (or simply sleeves) to be applied on the inner wall of the nozzle. These preforms allow to produce composite parts having a cylindrical symmetry and complex geometries with minimum efforts, maximizing the affordability and reliability of the manufacturing process. Once the size of a sleeve is selected, the preform can be deformed in a given range of diameters corresponding to a minimum and maximum degree of the fiber orientation. Commercial sleeves are generally available in different sizes (typically up to 25" for PAN-based carbon or E-glass fibers) and can be used to produce high pressure tank or to manufacture the nozzle assembly of solid rocket motors [61]. Braided preforms have to be generally impregnated with the proper infiltrant to meet the thermo-mechanical requirements of the part to be manufactured. In the application under study an elastomeric infiltrant such

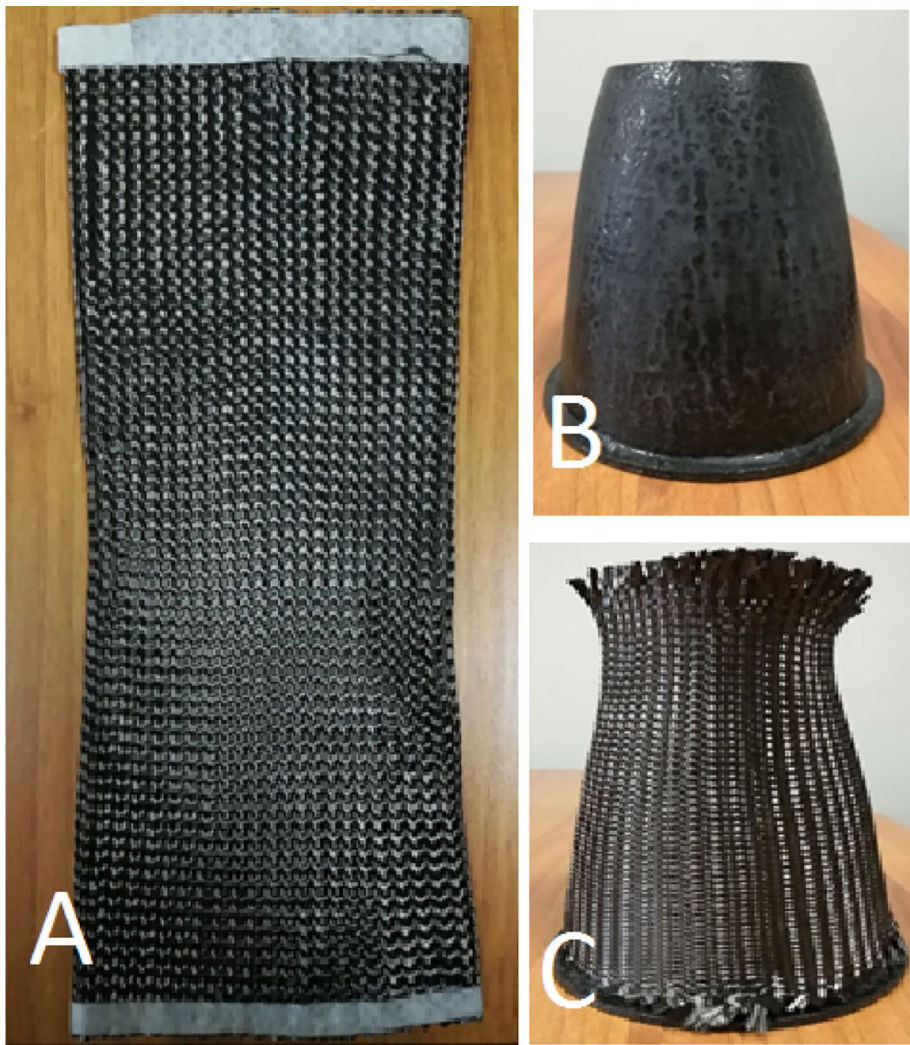


Fig. 14 Application of carbon fabric sleeves for internal coating of nozzles: carbon sleeve (A), nozzle-shaped mold (B), and application of the sleeve to the nozzle geometry (C)

as silicone could be candidate to produce the flexible TPS inner heat shield. Figure 14A shows a tubular sleeve, which can be shaped around a mold reproducing the nozzle shape (Fig. 14B), as indicated in Fig. 14C.

The considerations reported in this subsection suggest that alternative and innovative different technologies exist or are currently being studied to develop a lightweight TPS with adequate ablation properties and low stiffness values, which would lead to minimize the force required for actuation. In particular, the potential of new materials and technologies could improve the performances of the solutions which are presented in detail in the next section, which are however based on consolidated materials for the development of the FTPS.

5 Mechanical Performances of a Design Solution for a Selected Application Scenario

5.1 Selected Configuration and Development of a FE Model

The feasibility studies for the thermal protection of the corrugated sections completed the information required for a possible design hypothesis of the morphing nozzle concept proposed in this paper. A classical theory for shaping the nozzle contour [62, 63] was applied to identify the geometry of a morphing nozzle with 6 kN of thrust, a divergent length of 276 mm, a throat diameter of 38 mm and an exit diameter of 196 mm, with the same expansion ratio and propulsive parameters of AS1 case. As an example, this nozzle could be applied to develop an engine with TVC providing two times the thrust of the MR-80B MLE engine, considered in the AS1 and the availability of TVC could reduce the number of thrusters required for maneuvering the planetary lander in the original application. It can be observed that reference values for the thrust-to-weight ratio of an engine can be set to 90 without any TVC capability and to 55 for engines with TVC [64], but also that the concept proposed in the paper is expected to reduce the weight and the complexity required for the introduction of TVC.

The finite element model of the nozzle is presented in Fig. 15, where also the main geometrical parameters are provided. The model includes a rigid section, about 100 mm long, which was modelled by using rigid elements (*R3D4* type [39]). The morphing section starts from 36.1% of the divergent length and was designed considering two corrugated modules with mutually perpendicular lateral stiffeners and the same corrugated profile of the cylindrical demonstrator discussed in Sect. 2, modelled by using bi-linear laminated shell elements (*S4R* type [39]). A lay-up $_{45}^2$ made of fabric plies was considered, with the properties of the material used for the technological demonstrator. The total length of the morphing part is about 180 mm.

The lateral stiffeners were meshed as shown in Fig. 15B and modelled considering a 1.0 mm thick core in titanium alloy ($E=110000$ MPa, $\nu=0.3$), which was externally reinforced by two external layers of carbon fabric ply, oriented in the direction of the nozzle axis.

The model of the design solution was developed considering the need of studying different combination of materials and thicknesses for the FTPS systems, based on the scheme proposed in Fig. 11. The development of many different geometries and meshes was avoided by defining equivalent materials for the layers 1, 2 and 3, shown in Fig. 15B,

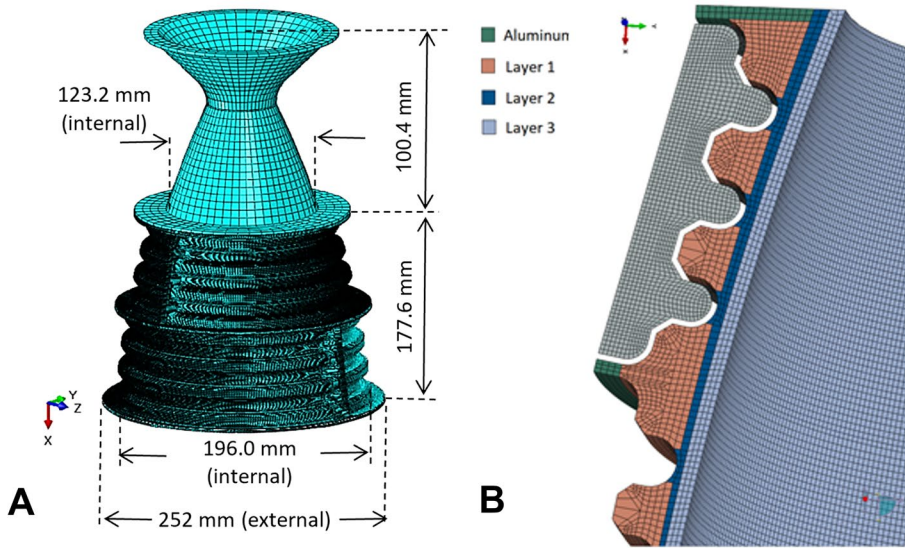


Fig. 15 Finite element model of the design solution (A) and detail of the lateral section in the morphing section in the three-layer version (B)

which represent the supporting filler in the corrugated valleys, the insulating layer, and the ablative layer, respectively.

All the versions evaluated in the numerical activity included the introduction of honeycomb stripes to support the FTPS in the valley of the corrugate nozzle, with a thickness $s_{honeycomb} = 12$ mm, which was modelled by 8-noded bricks (C3D8R type [39]) denoted as layer 1 in Fig. 15B. A silicon rubber cushion with a thickness $s_{rubber} = 1.5$ mm was included between the valleys of the corrugated laminate and the bottom of the honeycomb stripe, as shown in Fig. 11B, for the reasons discussed in subsection 4.2. Such a solution was modelled by means of an equivalent material for layer1, with Young modulus E_{eq1} , which was obtained by combining the stiffness of the honeycomb insert, with a modulus $E_{honeycomb}$ and a thickness $s_{honeycomb}$, and the one of the rubber cushion, with a modulus E_{rubber} and a thickness s_{rubber} . As shown in Eq. 6, the Young modulus E_{eq1} was evaluated by inverting the sum of the compliances per unit area of the honeycomb insert, $E_{honeycomb}/s_{honeycomb}$, and of rubber cushion, E_{rubber}/s_{rubber} both divided by the total thickness to obtain an equivalent material:

$$E_{eq1} = \frac{1}{\frac{1}{s_{honeycomb} + s_{rubber}} \frac{s_{rubber}}{E_{rubber}} + \frac{1}{s_{honeycomb} + s_{rubber}} \frac{s_{honeycomb}}{E_{honeycomb}}} \tag{6}$$

A value E_{rubber} of 0.45 MPa was considered for the silicon rubber cushion [27] and the application of Eq. 6 with such value and the honeycomb module provided in Table 3 led to $E_{eq1} = 4.04$ MPa. Hence, the orthotropic material data in Table 3 were used, with the substitution $E_{33} = E_{eq1}$, to characterize the filler material in layer 1 shown in Fig. 15B, considering the application of the rubber cushion.

The flexible protection made of ablative and/or insulating layers was modelled by using solid elements (C3D8R type [39]), considering a thickness linearly variable along the nozzle axis, $s_{FTPD}(x)$, starting from a thickness of 6.9 mm at the beginning of the morphing

section, until a thicknes of 3.9 mm at the end section of the nozzle. The thickness of FTPS in the model was indicative and single equivalent material, with a Young Modulus E_{eq2} was used to characterize all the elements of the FTPS denoted as layer2 and layer3 in Fig. 15B. This made possible modelling with a single FE mesh the mechanical response of a generic combination of materials and thickness for the insulating (layer 2) and ablative (layer 3) sub-layers, with Young moduli E_{Layer2} and E_{Layer3} , and also different thickness t_{Layer2} and t_{Layer3} , respectively. Assuming that the thickness fractions of the two sub-layers remained constant along the nozzle, first an equivalent modulus E_{FTPS} was evaluated considering the thickness fraction of the two layers in the initial section of the morphing nozzle, according a rule of mixture. Then the equivalent module E_{eq2} for the FE model was found by considering the ratio between the actual thickness of the FTPS in design hypothesis, t_{FTPS} , and the initial total thickness of the layers represent by solid elements in the finite element model, t_{Model} . The complete expression of E_{eq2} is given in Eq. 7.

$$E_{Eq2} = \frac{t_{FTPS}}{t_{Model}} E_{FTPS} = \frac{t_{FTPS}}{t_{Model}} \left(\frac{t_{layer2}}{t_{FTPS}} E_{layer2} + \frac{t_{layer3}}{t_{FTPS}} E_{layer3} \right) \tag{7}$$

Overall, the finite element model of the nozzle was developed with a total number of about 200,000 shell elements and more than 2 million of solid element. The mesh of solid elements and the shell mesh were connected through an algorithm provide by the solver code to join dissimilar mesh (*Tie* [39]). Such technique was also used to connect the morphing and the rigid parts of the nozzle as well as the edges of the lateral stiffeners to the corrugated profile. At the exit section, a rigid body was created with the element of the end flange. The application of a rigid rotation to such flange was intended to represent the action of an actuation system and the reaction moment evaluated the moment required for the morphing of the nozzle.

The load conditions consisted of an internal pressure field, which took into account both the pressure in the rigid nozzle for AS1 scenario, given in Fig. 3A, and an additional pressure field originated by the variation of velocity vector of the fluid. The pressure field for the rigid nozzle varies from 0.35 bar at the beginning of the morphing part until to 0.1 bar at the exit. It was interpolated by an exponential functions and applied to the internal surface of the ablative/insulating layer, as shown in Fig. 16A. The additional pressure field was evaluated in correspondence of a rotation of 9°, imposed to the rigid flange at

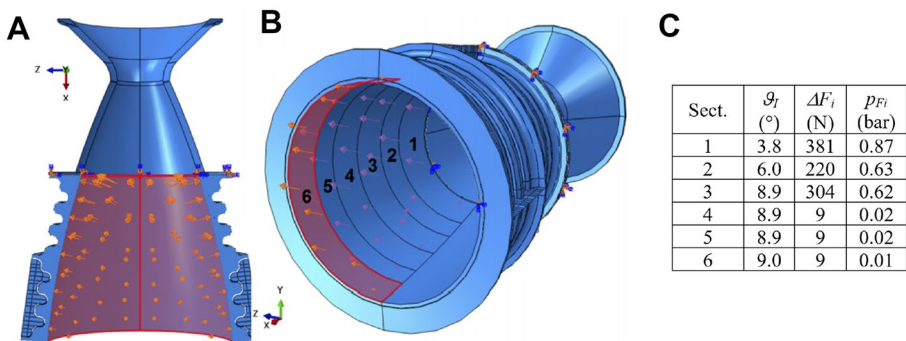


Fig. 16 Application of internal pressure fields: rigid nozzle pressure field (A), additional pressure field estimated for the variation of velocity direction (B), force and pressure values for a rotation of 9° about the y axis (C)

the nozzle exit. The morphing part of the nozzle was divided into six sections, shown in Fig. 16B and the rotation angles of the nozzle axis, ϑ_i , were estimated for each section. Considering the rotation of the fixed section $\vartheta_0 = 0$, the force ΔF_i , exerted by the fluid on each section was estimated as:

$$\Delta F_i = \dot{m}|\vec{v}| \sin(\vartheta_i - \vartheta_{i-1}) \quad i = 1, 2, \dots, 6 \quad (8)$$

where \dot{m} is the mass flow rate and the $|\vec{v}|$ is the magnitude of the gas exhaust velocity.

Such force was distributed as a constant pressure field acting on half of the circumference of the internal wall of the corresponding section, as shown in Fig. 16B. The table included in Fig. 16C referred to a rotation about the y axis, reports the values of the lateral force and of the corresponding pressure for each section. It can be observed that, due to the presence of the lateral stiffeners, the rotation is completely obtained in the first three sections.

5.2 Numerical Results

The rotation of 9° about y involves the deformation of the morphing part closest to the throat, where the internal pressure is higher and the thermal protection system is thicker. Accordingly, the highest stress values and moments required for morphing are expected. The FE analysis for such a rotation was performed for three configurations of the FTPS, corresponding to the three cases presented in Table 4. In particular, the thicknesses reported in Table 4 were applied by calculating the equivalent Young moduli through Eq. 7, where *layer2* represented the insulating cork layer, while *layer3* represented the ablative EPDM layer. As discussed in the previous subsection, these thickness values were considered referred to the initial section of the morphing nozzle. Following the FE model geometry, the FTPS thickness decreased linearly, until a value of 56% of the initial thickness at the nozzle exit. It has been already observed in Sect. 3 that the Young modulus adopted of the EPDM is the maximum among the responses reported in [51], which include filled compounds. For such a reason, such value was also considered an approximation for the Hybrid EDPM based composite with reduced ablation rate [49], adopted for AS2/B scenario.

The main results of the analyses are presented in Table 5, which reports the maximum values of stress in the corrugated composite skin, in the composite reinforcing plies applied to the lateral stiffeners, in the titanium alloy core of such stiffeners. Moreover, the moment to be applied to the flange for the actuation and the bending stiffness are presented.

The bending moments required for achieving a rotation of 9° increases with the stiffness of the FTPS system. The figures of the bending stiffness are between 38.7 Nm/deg and 46.5 Nm/deg, that is about 20 times higher than that estimated from the experiments reported in Sect. 3.4 for the technological demonstrator presented in Sect. 3. Though the model of the nozzle has a larger final diameter and a shorter length with respect to technological demonstrator presented in Sect. 3, such large difference can be attributed to the stiffness of the FTPS system. Indeed, the comparison of the results referred to AS2/B and AS1 indicates that adding 1 mm of EPDM layer led to a 20% increment of the moment required for actuation. As a reference, the torque required for a 330 mm diameter insulated flexbeam joint in [16] are between 180 Nm/deg and 237 Nm/deg, neglecting the internal aerodynamic torque, depending on the material used for insulation. If insulation was not considered the torque is reduced to 113 Nm/deg. Although the nozzles considered in [16] cannot be directly compared with the one modelled in the present work, these data confirm the great influence of the thermal protective system on the moment required for actuation.

Table 5 Mechanical response of the morphing nozzle model with different FTPS solutions

FTPS configuration	Corrugated Composite Skin			Lateral Stiffener composite layers		Titanium alloy Stiffener Max σ^{VM} (MPa)	Actuation Moment at 9° (Nm)	Bending Stiffness (Nm/deg)
	Max σ_{11} (MPa)	Min σ_{11} (MPa)	Max r_{12} (MPa)	Max σ_{11} (MPa)	Min σ_{11} (MPa)			
AS1 3.5 mm Cork	486.3	-504.2	100.6	262.8	-322.2	329.0	348.1	38.7
AS2/A 6.3 mm EPDM	630.8	-643.1	109.2	299.8	-337.4	343.9	530.1	58.9
AS2/B 3.5 mm Cork + 1 mm EPDM	563.0	-580.3	107.4	264.3	-320.7	326.9	418.5	46.5

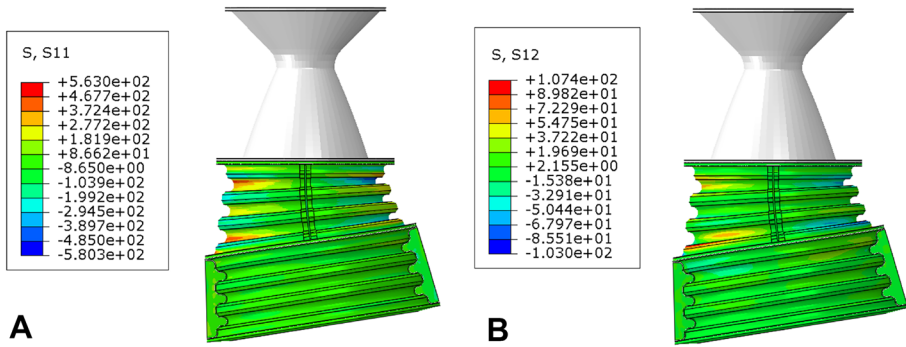


Fig. 17 Stress distribution in MPa on the composite skins in the AS2/B configuration for a rotation of 9°: normal stress σ_{11} (A), shear stress τ_{12} (B)

The maximum tensile normal stress in the composite skin are about 630 MPa, whereas the compressive one reaches a minimum of about –643 MPa. Such values are significant, though they are below the limits of many carbon-reinforced composite fabrics [40]. A maximum shear stress slightly higher than 100 MPa is obtained for all the considered configuration. Such value is close to the ultimate in-plane shear strength of typical carbon/epoxy composite plies, as be evaluated from the material data reported in [40].

The contours of normal and shear stress for AS2/B case are presented in Fig. 17. The qualitative distribution of the stress components is actually similar for all the three configurations presented. It can be observed that maximum values are obtained in the valleys of the first and last corrugations of the module rotated, while the central corrugation is subjected to lower stress values. A reinforcement in such zones, the optimization of the corrugated profile and of the load transmission between the lateral stiffeners and the flanges and between the flanges and the composite skin could lead to a mitigation of the peak stress and/or to an increment of the maximum rotation angle achievable.

The maximum principal strains in the solid elements representing the FTPS systems (layers 2 and 3 in Fig. 15B) are shown in Fig. 18 for the AS1 case, where only an insulating cork layer is considered (Fig. 18A), and in the AS2/A configuration (Fig. 18B), where the solid mesh represent a layer made of EPDM polymer. It can be seen that the maximum values are below the 25% elongation, that is lower than the maximum elongation levels presented in Table 3 for the cork and the EPDM compound, though they exceed the value of 12.1% declared for the hybrid EPDM with low ablation rate proposed in [49].

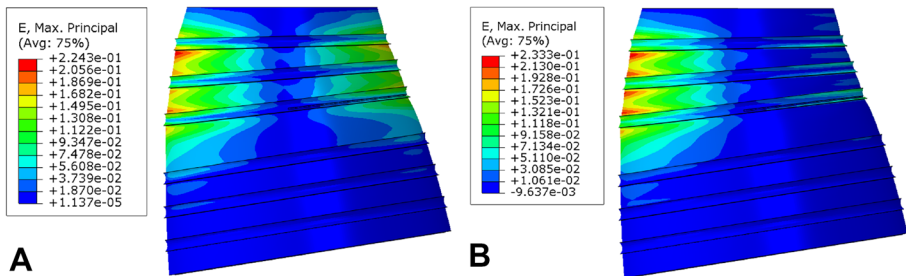


Fig. 18 Maximum principal strain in the FTPS layers for a rotation of 9°: AS1 scenario (A), AS2/A scenario (B)

The results reported in Table 5 also includes the stress components in the lateral stiffeners, which transmit the vertical resultant of the wall pressure to the rigid part of the nozzle and, at the same time, bend to accomplish the rotation. The stress values in both the composite reinforcements and in internal core, characterized by considering the properties of a Titanium alloy, are well below the elastic limits of the materials.

6 Concluding Remarks

The paper presented the possibility of exploiting the properties of composite corrugated laminates for the development of a morphing nozzle with thrust vector control. The structural concept was based on the separation of the load path involved in axial thrust transmission from the requirements related to the containment of internal pressures and to the control of the bending compliance, which are demanded to a corrugated composite skin. The structural concept and the technological feasibility of the required cylindrical corrugated shape by lamination of composite plies were successfully tested by developing a technological demonstrator, which was also exploited to validate a numerical approach. The challenges related to the protection from the hot exhaust plume were preliminary addressed by proposing systems conjugating insulation and ablation performances with flexibility and high elongation at failures. Solutions aimed at overcome the limitations of the flexible thermal protection system concepts studied in the paper were also proposed. The solutions obtained with the integration of such protective layers in the composite nozzle were evaluated numerically, by using material data collected through a survey of the open literature. Numerical models simulated the thermal transient in two different realistic application scenarios and made possible the definition of possible configurations for a flexible internal thermal protection system. Finally, the results of the technological, experimental and numerical activities were combined in a virtual model of the nozzle, which was analyzed under the action of all the mechanical loads originated by the internal pressures, the actuation moment required for deformation of the nozzle and the additional pressure field related to the deviation of the thrust vector. The results achieved indicated that the proposed concept is technologically feasible and that the stress and temperature levels in operational conditions can be maintained within adequate limits. Although several simplifying assumptions were introduced in the numerical evaluations, many of these simplifications were actually conservative, such as those related to the maximum working temperature of the composite skin and the stiffness of the EPDM compounds. Moreover, the corrugated profile and the overall structural design of the virtual configurations investigated were not optimized and there are margins to improve the mechanical performances of the system.

Overall, the concept appears promising, from the technological and functional standpoint, to develop a sacrificial morphing terminal section of a nozzle, characterized by relatively low complexity and cost with respect to the solutions currently adopted for thrust vector control. The capability of reaching rotation angles higher than those obtained in typical flexseal applications was assessed. The activities performed point out that the development of an ad hoc flexible thermal protection system represents a key aspect for the development of a successful application with lower complexity, cost and actuation torque with respect to the currently adopted technologies. Indeed, the specific operational conditions and requirements for such thermal protection system are characterized by lower pressures and temperature with respect to typical applications in propulsive systems, but also by higher gas velocities. Moreover, the flexibility of the thermal protection system greatly

affects the moment required for the actuation and has a direct impact on the power required for the actuation and the total weight. Finally, it has to be remarked, that the assessment of the technological feasibility of composite elements with high bending compliance and axial load bearing capability may be exploited to substitute more complex mechanisms where relative motions between structural elements is required, in application fields that could be different from the one investigated in this paper.

Acknowledgements The activities presented in this work received a partial financial support from project COMETAS (Cost Effective Material and Technologies for Access to Space) funded under the H2020-MANUNET (Ref. MNET17/NMCS-1177) initiative. The authors want to thank Stefano Losa for his help in the definition of application scenarios.

Funding Open access funding provided by Politecnico di Milano within the CRUI-CARE Agreement. The activities presented in this work received a partial financial support from project COMETAS (Cost Effective Material and Technologies for Access to Space) funded under the H2020-MANUNET (Ref. MNET17/NMCS-1177) initiative.

Availability of Data and Materials All the data generated during this study are available from the corresponding author on reasonable request.

Declarations

Conflicts of Interests The authors declare no conflict of interests.

Open Access This article is licensed under a Creative Commons Attribution 4.0 International License, which permits use, sharing, adaptation, distribution and reproduction in any medium or format, as long as you give appropriate credit to the original author(s) and the source, provide a link to the Creative Commons licence, and indicate if changes were made. The images or other third party material in this article are included in the article's Creative Commons licence, unless indicated otherwise in a credit line to the material. If material is not included in the article's Creative Commons licence and your intended use is not permitted by statutory regulation or exceeds the permitted use, you will need to obtain permission directly from the copyright holder. To view a copy of this licence, visit <http://creativecommons.org/licenses/by/4.0/>.

References

1. Boyce, R., Tirtay, S., Brown, L., Creagh, M., Ogawa, H.: SCRAMSPACE: scramjet-based access-to-space systems. In 17th AIAA International Space Planes and Hypersonic Systems and Technologies Conference. p. 2297. San Francisco, California (2011). <https://doi.org/10.2514/6.2011-229>
2. Smart, M.K., Tetlow, M.R.: Orbital delivery of small payloads using hypersonic airbreathing propulsion. *J. Spacecr. Rocket.* **46**(1), 117–125 (2009). <https://doi.org/10.2514/1.38784>
3. Dimotakis, P., Garwin, R., Katz, J., Vesecky, J.: 100 lbs to Low Earth Orbit (LEO): Small-Payload Launch Options. Mitre Corp Mclean Va Jason Program Office. (1999)
4. Cohen-Zur, A., Natan, B.: Experimental investigation of a supersonic combustion solid fuel ramjet. *J. Propul. Power* **14**(6), 880–889 (1998). <https://doi.org/10.2514/2.5379>
5. Sutton, G.P., Biblarz, O.: Rocket propulsion elements. John Wiley & Sons (2016)
6. French, J.R., Griffin, M.D.: Space vehicle design, pp. 231–236. AIAA Education Series, Washington, DC (1991)
7. Orientation, S.S.M.E.: Space Transportation System Training Data. BC98–04, Rocketdyne Propulsion & Power, Boeing (1998)
8. Haidn, O.J.: Advanced rocket engines. Advances on propulsion technology for high-speed aircraft **1**, 6–1 (2008)
9. Woodberry, R.F.H., Zeamer, R.J.: Solid rocket thrust vector control. NASA SP-8114, 4–17 (1974)
10. Wendel, G.M.: U.S. Patent No. 4649701. U.S. Patent and Trademark Office, Washington, DC (1987)

11. Berdoyes, M., Dauchier, M., Just, C.: A New Ablative Material Offering SRM Nozzle Design Breakthroughs. In 47th AIAA/ASME/SAE/ASEE Joint Propulsion Conference & Exhibit, p. 6052. San Diego, California (2011). <https://doi.org/10.2514/6.2011-6052>
12. Ram Mohan, C.H., Ramanathan, J., Kumar, S., Gupta, A.V.S.K.S.: Characterisation of Materials Used in Flex Bearings of Large Solid Rocket Motors. *Def. Sci. J.* 61(3), (2011). <https://doi.org/10.14429/dsj.61.52>
13. Descamps, C., Gautronneau, E., Rousseau, G., Daurat, M.: P80 SRM low torque flex-seal development—thermal and chemical modeling of molding process. *Progress in Propulsion Physics* 1, 141–152 (2009). <https://doi.org/10.1051/eucass/200901141>
14. Ren, J., Zhang, X., Yang, J., Wang, C., Liu, Y., Yang, W.: Structural analysis and testing of a miniature flexible joint under pressure and vector loading. *J. Mech. Sci. Technol.* 28(9), 3637–3643 (2014). <https://doi.org/10.1007/s12206-014-0825-8>
15. Lampani, L., Angelini, F., Bernabei, M., Marocco, R., Fabrizi, M., Gaundenzi, P.: Finite Element Analysis of a Solid Booster Flexible Bearing Joint for Thrust Vector Control. *Aerotecnica & Spazio, The Journal of Aerospace Science, Technology and Systems* 91(1), 2 (2012)
16. Douglass, H.W., Collins Jr, J.H., Ellis, R.A., Keller Jr, R.B.: Solid Rocket Motor Nozzles. NASA SP-8115 (1975)
17. Counter, D.N., Brinton, B.C.: Thrust vector control for the space shuttle solid rocket motor. In 11th AIAA Propulsion Conference (No. 75–1172). Anaheim, California (1975)
18. Caye, P., & Descamps, D.: Ariane 5 thrust vector control system development status. In 30th Joint Propulsion Conference and Exhibit, p. 3069. Indianapolis, Indiana (1994)
19. Barbarino, S., Bilgen, O., Ajaj, R.M., Friswell, M.I., Inman, D.J.: A review of morphing aircraft. *J. Intell. Mater. Syst. Struct.* 22(9), 823–877 (2011). <https://doi.org/10.1177/1045389X11414084>
20. Sofla, A.Y.N., Meguid, S.A., Tan, K.T., Yeo, W.K.: Shape morphing of aircraft wing: Status and challenges. *Mater. Des.* 31(3), 1284–1292 (2010). <https://doi.org/10.1016/j.matdes.2009.09.011>
21. Yokozeki, T., Takeda, S.I., Ogasawara, T., Ishikawa, T.: Mechanical properties of corrugated composites for candidate materials of flexible wing structures. *Compos. A Appl. Sci. Manuf.* 37(10), 1578–1586 (2006). <https://doi.org/10.1016/j.compositesa.2005.10.015>
22. Thill, C.L., Etches, J., Bond, I., Potter, K., Weaver, P.: Morphing skins. *The aeronautical journal* 112(1129), 117–139 (2008). <https://doi.org/10.1017/S0001924000002062>
23. Thill, C., Etches, J.A., Bond, I.P., Potter, K.D., Weaver, P.M.: Composite corrugated structures for morphing wing skin applications. *Smart Mater. Struct.* 19(12), 124009 (2010). <https://doi.org/10.1088/0964-1726/19/12/124009>
24. Winkler, M., Kress, G.: Influence of corrugation geometry on the substitute stiffness matrix of corrugated laminates. *Compos. Struct.* 94(9), 2827–2833 (2012). <https://doi.org/10.1016/j.compstruct.2012.03.008>
25. Xia, Y., Friswell, M.I., Flores, E.S.: Equivalent models of corrugated panels. *Int. J. Solids Struct.* 49(13), 1453–1462 (2012). <https://doi.org/10.1016/j.ijsolstr.2012.02.023>
26. Previtali, F., Molinari, G., Arrieta, A.F., Guillaume, M., Ermanni, P.: Design and experimental characterisation of a morphing wing with enhanced corrugated skin. *J. Intell. Mater. Syst. Struct.* 27(2), 278–292 (2016). <https://doi.org/10.1177/1045389X15595296>
27. Airoidi, A., Fournier, S., Borlandelli, E., Bettini, P., Sala, G.: Design and manufacturing of skins based on composite corrugated laminates for morphing aerodynamic surfaces. *Smart Mater. Struct.* 26(4), 045024 (2017). <https://doi.org/10.1088/1361-665X/aa6069>
28. Airoidi, A., Sala, G., Di Landro, L. A., Bettini, P., Gilardelli, A.: Composite corrugated laminates for morphing applications. In *Morphing Wing Technologies*, p. 247–276. Butterworth-Heinemann (2018). <https://doi.org/10.1016/B978-0-08-100964-2.00009-5>
29. Schmitz, A., Horst, P.: Bending deformation limits of corrugated unidirectionally reinforced composites. *Compos. Struct.* 107, 103–111 (2014). <https://doi.org/10.1016/j.compstruct.2013.07.048>
30. Dawson, M., Brewster, G., Conrad, C., Kilwine, M., Chenevert, B., Morgan, O.: Monopropellant hydrazine 700 lbf throttling terminal descent engine for Mars science laboratory. In 43rd AIAA/ASME/SAE/ASEE Joint Propulsion Conference & Exhibit, p. 5481. Cincinnati, Ohio (2007). <https://doi.org/10.2514/6.2007-5481>
31. Schmit, D.D., Anderson, J.W., Vote, F.C.: Long-life bipropellant system demonstration, viking orbiter propulsion system. *J. Spacecr. Rocket.* 18(4), 327–332 (1981). <https://doi.org/10.2514/3.57824>
32. Northrop Grumman, Propulsion Product Catalogue.: <https://www.northropgrumman.com/wp-content/uploads/NG-Propulsion-Products-Catalog.pdf>. Accessed on 21 Aug 2022.
33. McBride, B. J.: Computer program for calculating and fitting thermodynamic functions. National Aeronautics and Space Administration, Office of Management, Scientific and Technical Information Program. vol. 1271. (1992)

34. Adler, D., Dubrov, E., Manheimer-Timnat, Y.: The performance of a hydrazine engine with an improved catalyst. *Acta Astronaut.* **2**(7–8), 613–625 (1975). [https://doi.org/10.1016/0094-5765\(75\)90005-3](https://doi.org/10.1016/0094-5765(75)90005-3)
35. ASTM Standard D3039/D3039M-14.: Standard Test Method for Tensile Properties of Polymer Matrix Composite Materials. ASTM International, West Conshohocken, PA, (2014)
36. ASTM Standard D3518/D3518M – 13.: Standard Test Method for In-Plane Shear Response of Polymer Matrix Composite Materials by Tensile Test of a $\pm 45^\circ$. ASTM International, West Conshohocken, PA, (2013)
37. Hexply M49 Product Datasheet.: https://www.hexcel.com/user_area/content_media/raw/HexPly_M49_eu_DataSheet.pdf. Accessed on 14 Sept 2021
38. EOS GmbH, PA2200 Product Datasheet.: <https://eos.materialdatacenter.com/eo/en>. Accessed on 14 Sept 2021
39. Dassault Systemes Simulia Corporation.: Abaqus Analysis User Manual Version 6.12. (2012)
40. Department of Defense Handbook.: Composite materials handbook. Volume 3: polymer matrix composites materials usage, design, and analysis, MIL-HDBK-17–3F. Document Automation and Production Service (DAPS). (2002)
41. Tauzia, J. M.: Thermal insulations, liners and inhibitors. In *Solid rocket propulsion technology*. pp. 553–583. (1993). Pergamon Press. <https://doi.org/10.1016/B978-0-08-040999-3.50018-7>
42. Silva, J., Gamboa, P., Nunes, C., Paulo, L., Franco, N.: Cork: Is it a good material for aerospace structures? In *52nd AIAA/ASME/ASCE/AHS/ASC Structures, Structural Dynamics and Materials Conference 19th AIAA/ASME/AHS Adaptive Structures Conference 13th*, p. 2159. Denver, Colorado (2011). <https://doi.org/10.2514/6.2011-2159>
43. Smith, E., Laub, B., Beck, R., Fretter, E.: Thermal/ablation model of low density cork phenolic for the Titan IV Stage I engine thermal protection system. In *27th Thermophysics Conference*, p. 2905. Nashville, Tennessee (1992). <https://doi.org/10.2514/6.1992-2905>
44. Boehrk, H., Stokes, J.L.: Kinetic parameters and thermal properties of a cork-based material. In *20th AIAA International Space Planes and Hypersonic Systems and Technologies Conference*, p. 3532. Glasgow, Scotland (2015). <https://doi.org/10.2514/6.2015-3532>
45. Gul, J., Saleemi, A.R., Mirza, S., Feroze, N., Mansha, M.: Thermal and mechanical characteristics of cork filled insulation for aerospace applications. *Plast., Rubber Compos.* **39**(1), 28–32 (2010). <https://doi.org/10.1179/174328910X12608851832010>
46. Bhuvanewari, C.M., Kakade, S.D., Deuskar, V.D., Dange, A.B., Gupta, M.: Filled Ethylene-propylene Diene Terpolymer Elastomer as Thermal Insulator for Case-bonded Solid Rocket Motors. *Def. Sci. J.* **58**(1), 94 (2008)
47. Natali, M., Rallini, M., Puglia, D., Kenny, J., Torre, L.: EPDM based heat shielding materials for Solid Rocket Motors: A comparative study of different fibrous reinforcements. *Polym. Degrad. Stab.* **98**(11), 2131–2139 (2013). <https://doi.org/10.1016/j.polyimdeggradstab.2013.09.006>
48. Chen, R., Lu, S., Li, C., Ding, Y., Zhang, B., Lo, S.: Correlation analysis of heat flux and cone calorimeter test data of commercial flame-retardant ethylene-propylene-diene monomer (EPDM) rubber. *J. Therm. Anal. Calorim.* **123**(1), 545–556 (2016). <https://doi.org/10.1007/s10973-015-4900-x>
49. Ahmed, A.F., Hoa, S.V.: Thermal insulation by heat resistant polymers for solid rocket motor insulation. *J. Compos. Mater.* **46**(13), 1549–1559 (2012). <https://doi.org/10.1177/0021998311418850>
50. Deuri, A.S., Bhowmick, A.K., Ghosh, R., John, B., Sriram, T., De, S.K.: Thermal and ablative properties of rocket insulator compound based on EPDM. *Polym. Degrad. Stab.* **21**(1), 21–28 (1988). [https://doi.org/10.1016/0141-3910\(88\)90062-6](https://doi.org/10.1016/0141-3910(88)90062-6)
51. Hu, X., Gao, H., Zhou, X., Cui, Y., Ge, H.: A new approach to rubber reinforcement. *RSC Adv.* **4**(26), 13662–13668 (2014). <https://doi.org/10.1039/C3RA47537A>
52. Amorim cork composites, Ablative Thermal Protection, Since the beginning of space exploration, Brochure.: <http://www.amorimcorkcomposites.com/en-us/materials-applications/aerospace/>. Accessed 24 Oct 2017
53. Díaz-Parralejo, A., Cuerda-Correa, E.M., Macías-García, A., Sánchez-González, J., Díaz-Díez, M.: The excellent mechanical properties of cork: a novel approach through the analysis of contact stress. *International Scholarly Research Notices* (2014). <https://doi.org/10.1155/2014/898439>
54. Natali, M., Kenny, J.M., Torre, L.: Science and technology of polymeric ablative materials for thermal protection systems and propulsion devices: a review. *Progress in Material Science* **84**, 192–275 (2016). <https://doi.org/10.1016/j.pmatsci.2016.08.003>
55. Bergman, T.L., Incropera, F.P., Dewitt, D.P., Lavine, A.S.: *Fundamentals of heat and mass transfer*. John Wiley & Sons (2011)
56. Hexcel, Hexweb CR III product datasheet.: https://www.hexcel.com/user_area/content_media/raw/HexWeb_CRIII_DataSheet.pdf. Accessed on 19 Aug 2022

57. DeSain, J.D., Brady, B.B.: Thermal conductivity of liquid hydrazine (N₂H₄) at 293.2 Kelvin and 0.101 to 2.068 Megapascals. *J. Thermophys. Heat Trans.* **23**(4), 828–835. (2009). <https://doi.org/10.2514/1.38775>
58. Zhang, J., Zhi, S., Sun, B.: Estimation of thermophysical properties of solid propellants based on particle packing model. *Science China Technol. Sci.* **56**(12), 3055–3069 (2013). <https://doi.org/10.1007/s11431-013-5368-1>
59. Turchi, A., Bianchi, D., Thakre, P., Nasuti, F., Yang, V.: Radiation and roughness effects on nozzle thermochemical erosion in solid rocket motors. *J. Propul. Power* **30**(2), 314–324 (2014). <https://doi.org/10.2514/1.B34997>
60. Natali, M., Rallini, M., Puglia, D., Kenny, J., Torre, L.: An Armadillo Like Flexible Thermal Protection System for Inflatable Decelerators: A Novel Paradigm. *Macromol. Mater. Eng.* **299**(3), 379–390 (2014). <https://doi.org/10.1002/mame.201300267>
61. Canfield, A.: Braided carbon/carbon nozzle development. In 21st Joint Propulsion Conference, p. 1096. Monterey, California (1985). <https://doi.org/10.2514/6.1985-1096>
62. Rao, G.V.R.: Exhaust nozzle contour for optimum thrust. *Journal of Jet Propulsion* **28**(6), 377–382 (1958). <https://doi.org/10.2514/8.7324>
63. Rao, G.V.R.: Recent developments in rocket nozzle configurations. *ARS journal* **31**(11), 1488–1494 (1961). <https://doi.org/10.2514/8.5837>
64. Bruno, C., Czysz, P.A.: *Future spacecraft propulsion systems: enabling technologies for space exploration*. Springer Science & Business Media (2009)
65. Herbert, J.T., Kovitch, F.J., McCorkle, M.: U.S. Patent No. 3390899. Washington, DC: U.S. Patent and Trademark Office (1968)

Publisher's Note Springer Nature remains neutral with regard to jurisdictional claims in published maps and institutional affiliations.